Inverse sound source reconstruction by exterior spherical acoustical holography with model adaptation

Alexander Mattioli Pasqual, Vincent Martin

18TH INTERNATIONAL CONGRESS ON SOUND & VIBRATION
ICSV18
RIO DE JANEIRO
BRAZIL
10–14 JULY 2011

INVERSE SOUND SOURCE RECONSTRUCTION BY EXTERIOR SPHERICAL ACOUSTICAL HOLOGRAPHY WITH MODEL ADAPTATION

Alexander Mattioli Pasqual, Vincent Martin

Institut Jean le Rond d'Alembert (UMR 7190), UPMC Univ Paris 06, CNRS, 2 place de la Gare de Ceinture, 78210, Saint-Cyr-l'Ecole, France, e-mail: ampasqual@gmail.com

Spherical acoustical holography (SAH) can be used to reconstruct the 3D sound field from acoustic data on a spherical surface, called the hologram sphere. In exterior SAH, the hologram sphere encloses all the sound sources and free-field conditions are assumed. Then, the acoustic variables can be reconstructed at any point exterior to the smallest sphere surrounding the sources (called the source sphere) by using a radiation model written in terms of spherical Hankel functions and spherical harmonics. This work deals with the inverse problem of reconstructing the radial particle velocity on the source sphere from the sound pressure field on the hologram sphere. This requires prior knowledge of the position of the source sphere inside the hologram sphere; as far as possible, these spheres must be made concentric to simplify the reconstruction equations. If the relative position of the hologram and source spheres is not known, an estimated position must be used. This may yield an inadequate propagator, so that the acoustic velocity field is poorly reconstructed. This contribution discusses the role of the relative position of the spheres in inverse source reconstruction. In addition, some strategies to improve the radiation model by adapting the source position from the hologram data are investigated.

1. Introduction

Spherical acoustical holography (SAH) is an imaging technique to reconstruct a 3-D sound field from available data on a spherical surface (the "hologram sphere"), which requires a wave propagation model [1]. The reconstruction equations differ essentially whether the problem of interior or exterior SAH is dealt with. In interior SAH, the sound sources surround the acoustic domain, and thus they are located outside the hologram sphere. In exterior SAH, the sources are located inside the hologram sphere and free-field conditions are assumed, so that the acoustic field can be reconstructed at any point exterior to the smallest imaginary sphere surrounding the sources (the "source sphere"). This work deals with exterior SAH. In particular, we focus on the inverse problem of reconstructing the radial particle velocity on the source sphere from the sound pressure on the hologram sphere.

Since the sound pressure is known on a spherical surface, it is naturally subjected to spherical harmonic analysis [1, 2]. The spherical harmonics representation of a sound field depends on the position and orientation of the coordinate system, i.e., translations and rotations have significant effects on the expansion coefficients [3]. Moreover, unlike rotation of the coordinate axes, translating the origin also changes the number of harmonics that must be retained to obtain an accurate representa-

tion of the acoustic field. Some recent studies [4–6] have described the effects of the translation on the spherical harmonics decomposition of sound pressure fields, and proposed some cost functions to obtain an optimal decomposition center that minimizes the high-order spherical harmonics content, so that a more compact description of the acoustic field is obtained. However, these works do not deal explicitly with inverse sound source reconstruction.

In this paper, the origin of the coordinate system is the center of the source sphere. Clearly, its position inside the hologram sphere is a parameter of the radiation model, which is assumed to be known in conventional exterior SAH; as far as possible, the spheres must be made concentric in order to simplify the reconstruction equations. However, in practice, the source may not be precisely positioned inside the hologram sphere. If so, a nominal position can be used, which may degrade the holography results. This work investigates the effects of the source position on the inverse reconstruction of its radial particle velocity. In addition, we discuss some strategies to estimate the source position from the sound pressure field it radiates on the hologram sphere. The paper is organized as follows: Section 2 provides a description of the problem to be addressed. Section 3 deals with the spherical harmonic analysis of the pressure field on the hologram sphere with a given but arbitrary position of the decomposition center. Section 4 focuses on the reconstruction equations and on two cost functions that can be used to estimate the source position. Finally, Sec. 5 gives simulation results in order to illustrate the ideas presented throughout the paper.

From a general point of view, the problem addressed in this paper consists in adapting a parameter of a propagation model in order to minimize a given cost function. Here, the model describes the sound radiation from the source, and the parameter that is to be adapted is its position. If an adequate cost function is used, the optimal position leads to the lowest reconstruction error, which corresponds obviously to the real position of the source. It is worth mentioning that Martin *et al.* [7] applied this approach to a related acoustical problem, that of planar near-field acoustical holography with generalized impedance boundary conditions.

2. Problem description

Throughout this paper, a harmonic time dependence $\mathrm{e}^{-\iota\omega t}$ is assumed, where $\iota \equiv \sqrt{-1}$, ω is frequency, and t is time. Lower and upper case bold letters indicate vectors and matrices, respectively.

Let Γ_h and Γ_s be imaginary spheres with radius r_h and r_s, centered at C and O, respectively. They enclose all the sources in the acoustic domain, such as the hermetic compressor depicted in Fig. 1a. Γ_s is the smallest sphere surrounding the sources, which will be referred to as "source sphere". Also, let $\mathbb{P}$ be the space of continuous functions defined on Γ_h and $p(\mathbf{x}) : |\mathbf{x}| \geq r_s$ be the free-field sound pressure produced by the sources, where $\mathbf{x}$ is the position vector in relation to the origin O. The sound pressure is given only at $\mathbf{x}_h \in \Gamma_h$, which defines the "hologram sphere".

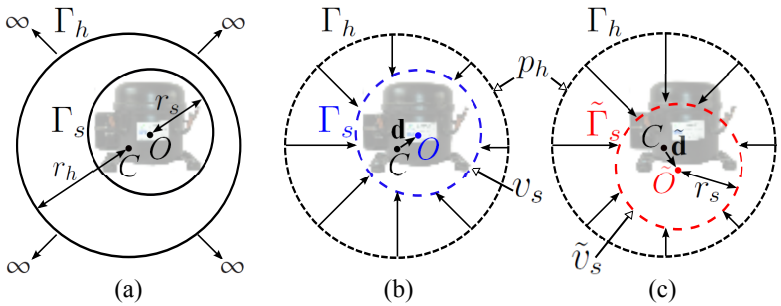

Figure 1: Illustration of the exterior SAH: (a) Two imaginary spheres Γ_h and Γ_s enclose a source that radiates under free-field conditions; (b) **d** known: The radial particle velocity (v_s) on Γ_s is reconstructed from the sound pressure (p_h) on Γ_h; (c) **d** unknown: The radial particle velocity ($\tilde{v}_s$) on a translated sphere $\tilde{\Gamma}_s$ is reconstructed from p_h and a nominal source position ($\tilde{\mathbf{d}}$).

Exterior SAH can be used to reconstruct the sound field at any point exterior to or on Γ_s from $p_h \equiv p(\mathbf{x}_h) \in \mathbb{P}$. In particular, we are interested in the inverse problem of determining the radial particle velocity $v_s \equiv v(\mathbf{x}_s) : \mathbf{x}_s \in \Gamma_s$, as shown in Fig. 1b, where $\mathbf{d} \equiv \overrightarrow{CO}$. This requires a radiation model that satisfies the Helmholtz equation and the geometrical configuration of the problem. Since $\mathbf{d}$ is clearly a parameter of the model, it must be known a priori. As far as possible, the sources position must be set so that Γ_h and Γ_s are concentric ($\mathbf{d} = \mathbf{0}$) to simplify the reconstruction equations. However, in practice, the sources may not be precisely positioned inside the hologram sphere. If so, a nominal position $\tilde{\mathbf{d}} \equiv \overrightarrow{C\tilde{O}}$ can be used in the holographic reconstruction, which leads to the radial particle velocity ($\tilde{v}_s$) on a translated source sphere ($\tilde{\Gamma}_s$), as illustrated in Fig. 1c. $\tilde{\Gamma}_s$ will be referred to as "equivalent source sphere". This work investigates the effects of $\delta\mathbf{d} \equiv \mathbf{d} - \tilde{\mathbf{d}}$ on the inverse sound source reconstruction, as well as some strategies to estimate $\mathbf{d}$ from a given p_h.

3. Spherical harmonic analysis of the sound pressure field

Let $r \geq 0$, $0 \leq \theta \leq \pi$, and $0 \leq \phi < 2\pi$ be spherical coordinates. Accordingly, the position vector is $\tilde{\mathbf{x}} = r\sin\theta\cos\phi\mathbf{e}_x + r\sin\theta\sin\phi\mathbf{e}_y + r\cos\theta\mathbf{e}_z$, where $\mathbf{e}_x$, $\mathbf{e}_y$, and $\mathbf{e}_z$ are the versors of the Cartesian coordinate system centered at the origin $\tilde{O}$. If the equivalent source sphere in Fig. 1c has a number sufficiently large of degrees of freedom, it is able to produce a given sound pressure field p_h on Γ_h regardless of $\tilde{\mathbf{d}}$. The sound pressure it radiates, $\tilde{p}(\tilde{\mathbf{x}}) : |\tilde{\mathbf{x}}| \geq r_s$, can be written as [1]

$$\tilde{p}(\tilde{\mathbf{x}}) = \sum_{n=0}^{N}\sum_{m=-n}^{n} C_n^m(\omega,\tilde{\mathbf{d}})h_n(kr)Y_n^m(\theta,\phi) = \sum_{n=0}^{N}\sum_{m=-n}^{n} \gamma_n^m(r,\tilde{\mathbf{d}})Y_n^m(\theta,\phi), \tag{1}$$

where k is the wave number, C_n^m are expansion coefficients, h_n are the spherical Hankel functions of the first kind, Y_n^m are the spherical harmonics, and

$$\gamma_n^m(r,\tilde{\mathbf{d}}) = C_n^m(\omega,\tilde{\mathbf{d}})h_n(kr) \tag{2}$$

is the so-called "spherical wave spectrum" of $\tilde{p}$ on a sphere defined by $|\tilde{\mathbf{x}}| = r$ [1]. Note that C_n^m are obtained from p_h, and thus they depend on $\tilde{\mathbf{d}}$.

Here, we only deal with band-limited functions, i.e., $C_n^m = 0$ if $n > N$, so that the series has $N' \equiv (N+1)^2$ terms. In fact, the order N required to ensure that $\tilde{p}(\tilde{\mathbf{x}}_h) = p_h : \tilde{\mathbf{x}}_h \in \Gamma_h$ depends on $\tilde{\mathbf{d}}$ in a difficult to predict way [3–6]. In this work, N is made large enough so that $\tilde{p}(\tilde{\mathbf{x}}_h) \approx p_h$ for the whole $\tilde{\mathbf{d}}$ range considered. Clearly, if $\tilde{\mathbf{d}} = \mathbf{d}$, one has $\tilde{p}(\tilde{\mathbf{x}}) = \tilde{p}(\mathbf{x}) \approx p(\mathbf{x}) : |\mathbf{x}| \geq r_s$.

3.1 Concentric spheres

It is known that Y_n^m are orthonormal functions over the unit sphere (see, e.g., Ref. [2]). Therefore, if Γ_h and $\tilde{\Gamma}_s$ are concentric ($\tilde{\mathbf{d}} = \mathbf{0}$), the expansion coefficients in Eq. (1) are given by

$$C_n^m(\omega,\mathbf{0}) = \frac{1}{h_n(kr_h)}\int_0^{\pi}\int_0^{2\pi} p_h Y_n^m(\theta,\phi)^* \sin\theta \mathrm{d}\theta\mathrm{d}\phi, \tag{3}$$

where the asterisk indicates complex conjugate.

Since C_n^m depends on frequency and $|h_n|$ increases rapidly with n for small arguments, it is helpful to use the set of coefficients $\gamma_n^m(r_h,\mathbf{0})$, which is the spherical wave spectrum of p_h. In this case, the Parseval's theorem,

$$\int_0^{\pi}\int_0^{2\pi} |p_h|^2 \sin\theta \mathrm{d}\theta\mathrm{d}\phi = \sum_{n=0}^{\infty}\sum_{m=-n}^{n} |\gamma_n^m(r_h,\mathbf{0})|^2 \approx \sum_{n=0}^{N}\sum_{m=-n}^{n} |\gamma_n^m(r_h,\mathbf{0})|^2, \tag{4}$$

shows that γ_n^m rather than C_n^m gives the contribution of the mode nm to the total energy of p_h.

3.2 Non-concentric spheres

For the sake of notation convenience, it is useful to combine the coefficients C_n^m into the column vector $\mathbf{c} \in \mathbb{C}^{N'}$, and the functions $h_n(kr)Y_n^m(\theta,\phi)$ into the column vector $\mathbf{s}(\tilde{\mathbf{x}})$, so that $c_i \equiv C_n^m$ and $s_i(\tilde{\mathbf{x}}) \equiv h_n(kr)Y_n^m(\theta,\phi)$, with $i = n^2+n+m+1$ for linear indexing. Then, Eq. (1) becomes

$$\tilde{p}(\tilde{\mathbf{x}}) = \mathbf{s}(\tilde{\mathbf{x}})^{\mathrm{T}}\mathbf{c}. \tag{5}$$

If $\tilde{\mathbf{d}} \neq \mathbf{0}$, the sphere Γ_h is described by a radial coordinate, r, that depends on (θ,ϕ). As a consequence, unlike for $\tilde{\mathbf{d}} = \mathbf{0}$, there is not a simple integral to evaluate c_i because s_i are not orthogonal over Γ_h. In this case, $\mathbf{c}$ can be obtained by solving the least-squares minimization problem,

$$\min_{\hat{\mathbf{c}}} R(\hat{\mathbf{c}}) = \min_{\hat{\mathbf{c}}} ||\mathbf{s}(\tilde{\mathbf{x}}_h)^{\mathrm{T}}\hat{\mathbf{c}} - p_h||, \tag{6}$$

where $\hat{\mathbf{c}} \in \mathbb{C}^{N'}$, $||\cdot|| = \langle\cdot\,,\cdot\rangle^{1/2}$ is the 2-norm, $\langle\cdot\,,\cdot\rangle$ is the inner product, and R is the residual norm. Throughout the paper, the norms and inner products of $\mathbb{P}$ and $\mathbb{C}^{N'}$ will be denoted by $||\cdot||$ and $\langle\cdot\,,\cdot\rangle$. We omit indices indicating the space because it will become clear from the context.

Problem (6) is convex and has an analytical solution given by

$$\mathbf{c} = \mathbf{A}^{-1}\mathbf{b}, \tag{7}$$

where $\mathbf{A} \in \mathbb{C}^{N'\times N'}$ with $A_{ij} = \langle s_j(\tilde{\mathbf{x}}_h), s_i(\tilde{\mathbf{x}}_h)\rangle$, and $\mathbf{b} \in \mathbb{C}^{N'}$ with $b_i = \langle p_h, s_i(\tilde{\mathbf{x}}_h)\rangle$.

Notice that, for low frequencies and large N, the matrix $A_{ij} = \langle s_j(\tilde{\mathbf{x}}_h), s_i(\tilde{\mathbf{x}}_h)\rangle$ is ill-conditioned due to the very different decay rates of h_n. In order to overcome this difficulty, $\gamma_n^m(r_h,\tilde{\mathbf{d}})$ can be used instead of C_n^m. In matrix/vector notation, Eq. (2) becomes

$$\boldsymbol{\gamma} = \mathbf{H}\mathbf{c}, \tag{8}$$

where $\mathbf{H} \in \mathbb{C}^{N'\times N'}$ is a diagonal matrix with $H_{ii} \equiv h_n(kr_h)$, and $\gamma_i \equiv \gamma_n^m(r_h,\tilde{\mathbf{d}})$, $i = n^2+n+m+1$. Then, by letting $\hat{\boldsymbol{\gamma}} \equiv \mathbf{H}\hat{\mathbf{c}}$, substitution of Eq. (8) into problem (6) leads to

$$\min_{\hat{\boldsymbol{\gamma}}} R(\hat{\boldsymbol{\gamma}}) = \min_{\hat{\boldsymbol{\gamma}}} ||\mathbf{s}(\tilde{\mathbf{x}}_h)^{\mathrm{T}}\mathbf{H}^{-1}\hat{\boldsymbol{\gamma}} - p_h||, \tag{9}$$

whose solution is given in Eq. (7), with $\boldsymbol{\gamma} = \hat{\boldsymbol{\gamma}}^{\mathrm{opt}} = \mathbf{A}^{-1}\mathbf{b}$, $A_{ij} = \left\langle s_j(\tilde{\mathbf{x}}_h)H_{jj}^{-1}, s_i(\tilde{\mathbf{x}}_h)H_{ii}^{-1}\right\rangle$, and $b_i = \left\langle p_h, s_i(\tilde{\mathbf{x}}_h)H_{ii}^{-1}\right\rangle$.

For $r_h >> |\tilde{\mathbf{d}}|$, the arguments of the spherical Hankel functions in $\mathbf{H}$ and $\mathbf{s}(\tilde{\mathbf{x}}_h)$ are nearly the same. If so, $\tilde{\mathbf{d}}$ has no appreciable effects on the conditioning of problem (9), which is well-posed.

4. Reconstruction of the radial particle velocity

4.1 Reconstruction equation

The solution of problem (9) leads to $\gamma_n^m(r_h,\tilde{\mathbf{d}})$. Then, $\tilde{v}_s$ can be calculated by [1]

$$\tilde{v}_s = \frac{1}{\iota\rho c}\sum_{n=0}^{N}\sum_{m=-n}^{n}\frac{h_n'(kr_s)}{h_n(kr_h)}\gamma_n^m(r_h,\tilde{\mathbf{d}})Y_n^m(\theta,\phi) = \sum_{n=0}^{N}\sum_{m=-n}^{n}\psi_n^m(r_s,\tilde{\mathbf{d}})Y_n^m(\theta,\phi), \tag{10}$$

where ρc is the characteristic impedance of the fluid, h_n' is the first derivative of h_n,

$$\psi_n^m(r_s,\tilde{\mathbf{d}}) = \frac{1}{\iota\rho c}\frac{h_n'(kr_s)}{h_n(kr_h)}\gamma_n^m(r_h,\tilde{\mathbf{d}}) \equiv \frac{1}{\iota\rho c}G_n\left(kr_s,\frac{r_h}{r_s}\right)\gamma_n^m(r_h,\tilde{\mathbf{d}}) \tag{11}$$

is the spherical wave spectrum of $\tilde{v}_s$, and G_n is the inverse propagator.

Figure 2 shows $|G_n|$ as a function of kr_s for $r_h/r_s = 2, 4,$ and 6. It can be noticed that $|G_n|$ increases significantly as kr_s decreases, and n and r_h/r_s increase. Therefore, inverse sound source reconstruction is usually an ill-posed problem, i.e., small measurement errors on p_h (and thus on $\gamma_n^m(r_h, \mathbf{d})$) can be greatly amplified, so that large errors may occur on the reconstructed velocity. This can be dealt with by using a low-pass filter in the spherical harmonic domain [8], which, however, reduces the spatial resolution of the reconstructed velocity field.

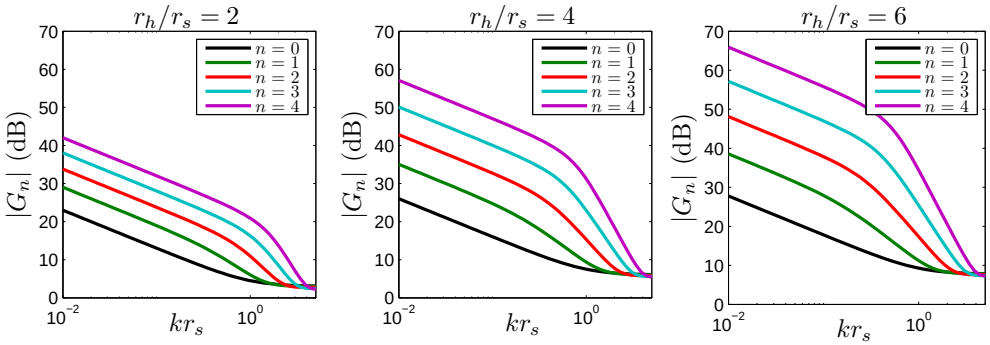

Figure 2: Inverse propagator up to order $n = 4$ as a function of kr_s for $r_h/r_s = 2, 4,$ and 6.

In this work, it is assumed that p_h is free from errors and that G_n can be accurately evaluated in a digital computer. Thus, if $\tilde{\mathbf{d}} = \mathbf{d}$, one has $\tilde{v}_s = v_s$ with no need of low-pass filtering. It is worth noting that, unlike measurement errors, the use of a nominal $\tilde{\mathbf{d}} \neq \mathbf{d}$ leads to biased errors on the reconstructed field, so that they cannot be reduced by low-pass filtering. In the following, we discuss two cost functions that can be used to estimate $\mathbf{d}$ from p_h, and thus to reduce such biased errors.

4.2 Model parameter estimation

As stated before, the number of spherical harmonics required to accurately describe p_h depends on $\tilde{\mathbf{d}}$. As $|\delta\mathbf{d}| = |\mathbf{d} - \tilde{\mathbf{d}}|$ increases, more terms must be retained in the spherical harmonic expansion [4, 6]. Thus, the minimal point of a cost function that penalizes high-order harmonics can be a good estimation of $\mathbf{d}$. This paper investigates the following two cost functions:

$$J_1(\tilde{\mathbf{d}}) = \frac{\sum_{n=0}^{N} n \sum_{m=-n}^{n} |\psi_n^m(r_s, \tilde{\mathbf{d}})|^2}{\sum_{n=0}^{N} \sum_{m=-n}^{n} |\psi_n^m(r_s, \tilde{\mathbf{d}})|^2}, \tag{12}$$

and

$$J_2(\tilde{\mathbf{d}}) = 1 - \frac{\sum_{n=0}^{\bar{N}} \sum_{m=-n}^{n} |\psi_n^m(r_s, \tilde{\mathbf{d}})|^2}{\sum_{n=0}^{N} \sum_{m=-n}^{n} |\psi_n^m(r_s, \tilde{\mathbf{d}})|^2}. \tag{13}$$

Because of the factor n in the summation, J_1 increases significantly as the contribution of high-order spherical harmonics increases. Unlike J_1, J_2 requires a cut-off order $\bar{N} < N$, so that this function measures the contribution of the spherical harmonics of orders $n > \bar{N}$; note that $0 \leq J_2 \leq 1$. J_2 would benefit from prior knowledge of the spatial resolution of the source velocity pattern, so that $\bar{N}$ could be easily determined. In this case, $J_2 = 0$ if $\tilde{\mathbf{d}} = \mathbf{d}$.

These cost functions were proposed by Rafaely [4] in order to evaluate the spectral changes in the pressure field due to translation of the coordinate system, and thus this author formulated them in terms of γ_n^m instead of ψ_n^m. Since we are interested in reconstructing the velocity field on a source sphere whose radius is known, it is more natural to use ψ_n^m for the purposes of this work.

5. Simulation results

In order to illustrate the ideas discussed throughout the paper, this section presents simulation results corresponding to a source sphere (Γ_s) of radius r_s placed at $\mathbf{d} = (0, 0, 0.1r_s)$. We investigate four axisymmetric velocity fields (v_s) on Γ_s with the following wave spectra ($\psi_n^m = 0$ if not specified):

(a) $\psi_0^0 = 1$;

(b) $\psi_1^0 = 1$;

(c) $\psi_0^0 = 1$, $\psi_1^0 = 0.3$, $\psi_2^0 = 0.1$;

(d) $\psi_0^0 = 0.2$, $\psi_1^0 = 1$, $\psi_4^0 = 0.1$.

Figure 3 shows these radial velocity fields, where the shape and the color map indicate, respectively, the amplitude and phase (in degrees) of v_s. Notice that the vertical axis, z, is the symmetry axis.

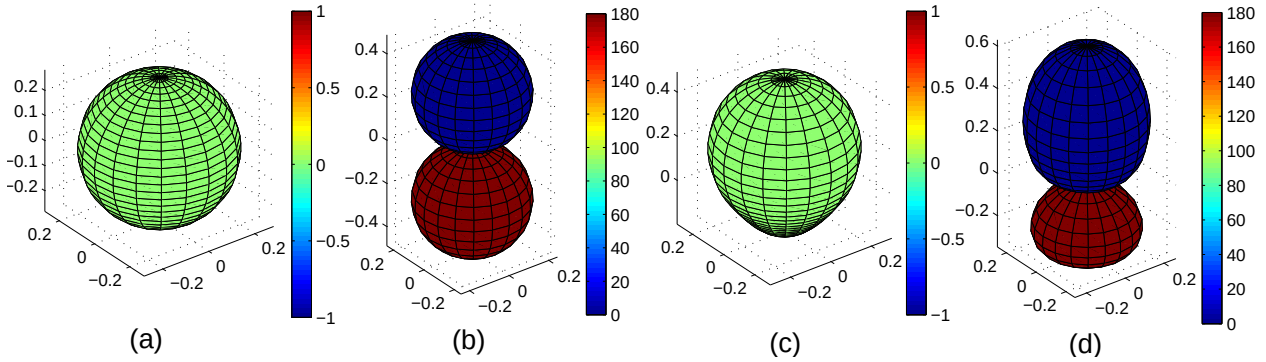

Figure 3: Axisymmetric radial velocity fields (v_s) on Γ_s. The shape and the color map indicate, respectively, the amplitude and phase (in degrees) of v_s.

To obtain the "measured" pressure fields (p_h) on Γ_h corresponding to the velocity fields shown in Fig. 3, we let $\rho c = 415\text{kg.m}^{-2}\text{.s}^{-1}$ and $r_h = 2r_s$. Two different kr_s values are considered: $kr_s = 0.1$ and $kr_s = 5$.

For the inverse problem of determining $\tilde{v}_s$ from p_h, we only deal with points $\tilde{O}$ located on the z axis due to the axisymmetry of p_h. Therefore, only positions given by $\tilde{\mathbf{d}} = (0, 0, z_s)$ are considered here. In addition, we let $N = 11$ in the spherical harmonics decomposition of p_h (problem (9)) — we have observed that this value ensures that $||\tilde{p}(\tilde{\mathbf{x}}_h) - p_h|| < 0.001||p_h||$ for the whole $\tilde{\mathbf{d}}$ range considered, namely, $-0.5r_s \leq z_s \leq 0.5r_s$. Since the spherical harmonics with $m \neq 0$ are not axisymmetric, only the harmonics with $m = 0$ are taken into account, which greatly reduces the computational cost because we deal with $N+1$ instead of $(N+1)^2$ functions. Finally, the usual inner product of $\mathbb{P}$ is approximately evaluated from 30 samples, which correspond to the co-latitudinal circumferences shown in Fig. 3. Area weighted factors are applied to the samples in order not to privilege densely sampled regions on the sphere.

Figure 4 shows the normalized least-square error ($||\tilde{v}_s - v_s||/||v_s||$) in velocity reconstruction, as well as the cost functions J_1 and J_2 (cut-off order $\bar{N} = 2$) as functions of z_s. These results correspond to the velocity fields shown in Fig. 3 for $kr_s = 0.1$ and $kr_s = 5$. The vertical dotted line indicates the real position of the source sphere.

The results reveal that even a small $\delta\mathbf{d}$ leads to a large error in the reconstructed velocity, so that $\tilde{\mathbf{d}}$ is a very important parameter of the radiation model. For $kr_s = 0.1$, the global minimal point of J_1 occurs at: (a) $z_s = 0.1r_s$, (b) $z_s = 0.1r_s$, (c) $z_s = 0.34r_s$, and (d) $z_s = 0.1r_s$. Similarly, the global minimal point of J_2 occurs at: (a) $z_s = 0.1r_s$, (b) $z_s = 0.1r_s$, (c) $z_s = 0.1r_s$, and (d) $z_s = 0.09r_s$. Thus, J_1 and J_2 give the correct source position for the cases (a) and (b). For the case (c), unlike J_2,

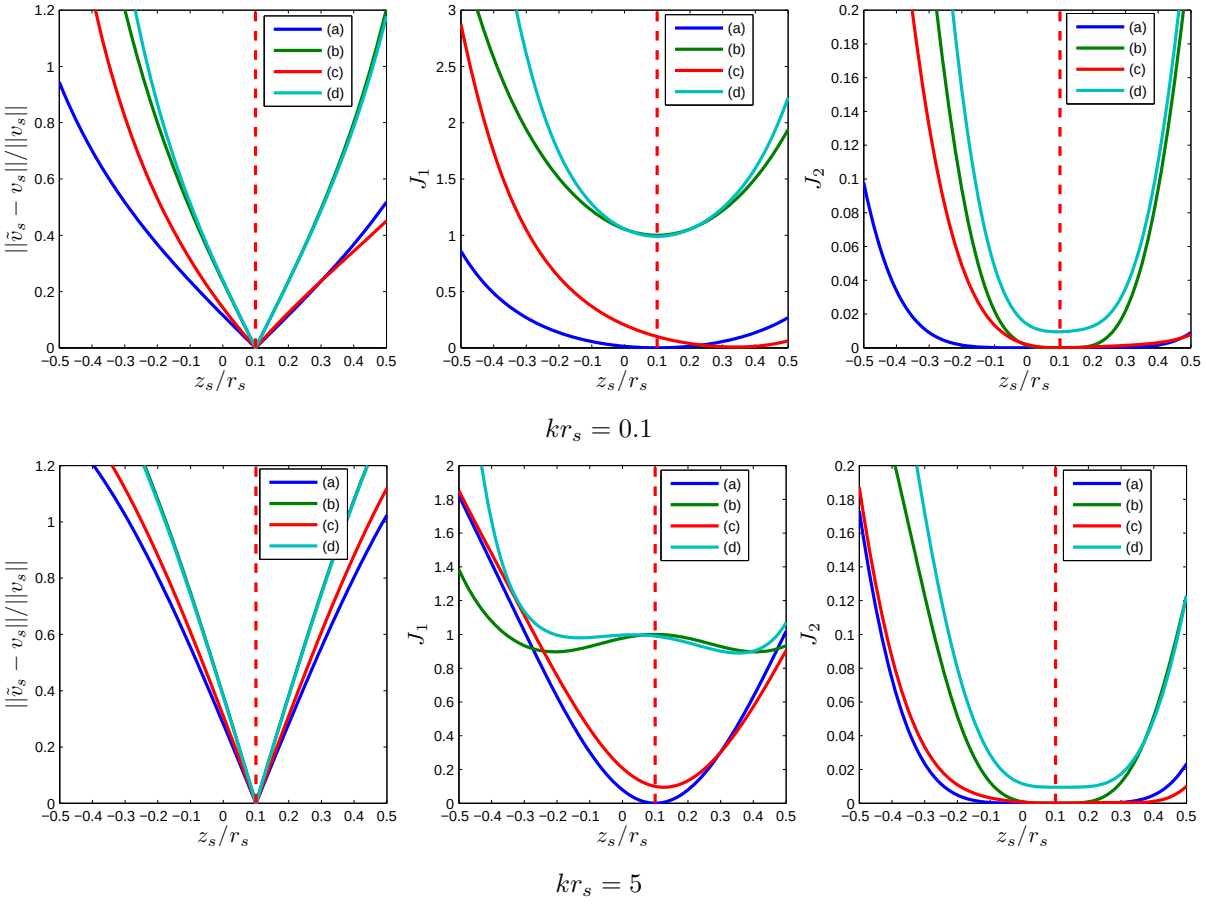

Figure 4: Error in velocity reconstruction ($||\tilde{v}_s - v_s||/||v_s||$), and cost functions J_1 and J_2 (cut-off order $\bar{N} = 2$) as functions of z_s. Results corresponding to the real velocity fields shown in Fig. 3 for $kr_s = 0.1$ and $kr_s = 5$. The vertical dotted line indicates the real position of the source sphere.

J_1 fails significantly. For the case (d), J_1 is able to correctly identify the source position, whereas J_2 leads to a small error.

For $kr_s = 5$, the global minimal point (or points) of J_1 occurs at: (a) $z_s = 0.1r_s$, (b) $z_s = (-0.21, 0.41)r_s$, (c) $z_s = 0.13r_s$, and (d) $z_s = 0.35r_s$. For J_2, it occurs at $z_s = 0.1r_s$ in the four cases under study. The source position is now easily identified for the case (a) by J_1, but this cost function fails for the remaining cases. Nevertheless, for the case (c), the "high-frequency" ($kr_s = 5$) simulations lead to an optimal position that is closer to the real position of the source sphere when compared to the "low-frequency" simulations ($kr_s = 0.1$). For the case (b) (dipole source), the real position of the source corresponds to a local maximum point of J_1, which is located between its two symmetrical global minima. This has also been observed by Deboy [5]. Unlike J_1, J_2 presents a similar behavior at low and high frequencies. Note that $J_2(0.1r_s) = 0$ for the cases (a), (b), and (c). This is due to the fact that the chosen cut-off order ($\bar{N} = 2$) is larger than or equal to the spatial resolution of the source, whereas $J_2(0.1r_s) > 0$ for the case (d).

The results show that using J_1 to identify the source position might lead to very large errors in inverse source reconstruction. On the other hand, if $\bar{N}$ is properly set, the real position of the source is ensured to be a minimal point of J_2. However, J_2 is less sensitive to z_s than J_1 in the neighborhood of the real position. Hence, in practice, J_2 cannot be sufficiently robust to identify the source position.

6. Conclusion

This paper has addressed the issue of inverse sound source reconstruction by exterior SAH. In particular, the effects of the source position on the reconstructed velocity field have been studied. In addition, we have investigated two cost functions to estimate the position of the source sphere from the sound pressure it radiates on the hologram sphere.

It has been shown that using a nominal position with a small deviation from the real position leads to large errors in the reconstructed velocity field. Thus, the position of the source sphere inside the hologram sphere must be precisely known in order to produce meaningful results. However, the cost functions investigated here are not always able to accurately identify the source position. Hence, the discussion of source position identification based on spherical harmonic analysis is left open for future work.

References

[1] E. G. Williams, *Fourier Acoustics: Sound Radiation and Nearfield Acoustical Holography*. London: Academic Press, 1999.

[2] G. B. Arfken and H. J. Weber, *Mathematical Methods for Physicists*, ch. 12, pp. 739–815. San Diego, CA: Harcourt/Academic Press, 5th ed., 2001.

[3] N. A. Gumerov and R. Duraiswami, "Recursions for the computation of multipole translation and rotation coefficients for the 3-D Helmholtz equation," *SIAM J. Sci. Comput.*, vol. 25, no. 4, pp. 1344–1381, 2003.

[4] B. Rafaely, "Spatial alignment of acoustic sources based on spherical harmonics radiation analysis," in *Proceedings of the 4th International Symposium on Communications, Control and Signal Processing*, (Limassol, Cyprus), pp. 1–5, Mar. 2010.

[5] D. Deboy, *Acoustic centering and rotational tracking in surrounding spherical microphone arrays*. Diploma thesis, University of Music and Performing Arts, Institute of Electronic Music and Acoustics, Graz, Austria, 2010. available at http://iem.at/Members/zotter (date last viewed 3/22/11).

[6] D. Deboy and F. Zotter, "Acoustic center and orientation analysis of sound-radiation recorded with a surrounding spherical microphone array," in *Proceedings of the 2nd International Symposium on Ambisonics and Spherical Acoustics*, (Paris), pp. 1–6, May 2010.

[7] V. Martin, T. Le Bourdon, and A. M. Pasqual, "Numerical simulation of acoustic holography with propagator adaptation: Application to a 3D disc," *Journal of Sound and Vibration*, 2011. (accepted for publication).

[8] E. G. Williams, "Regularization methods for near-field acoustical holography," *J. Acoust. Soc. Am.*, vol. 110, pp. 1976–1988, Oct. 2001.